Geometry-Based Thick Origami Simulation

Tsz-Ho Kwok
Department of Mechanical, Industrial and Aerospace Engineering
Concordia University
Montreal, QC H3G 1M8, Canada
Email: tszho.kwok@concordia.ca

Origami is the art of creating a three-dimensional (3D) shape by folding paper. It has drawn much attention from researchers, and the designs that origami has inspired are used in various engineering applications. Most of these designs are based on familiar origami patterns and their known deformations, but origami patterns were originally intended for materials of near-zero thickness, primarily paper. To use the designs in engineering applications, it is necessary to simulate origami in a way that enables designers to explore and understand the designs while taking the thickness of the material to be folded into account. Because origami is primarily a problem in geometric design, this paper develops a geometric simulation for thick origami. The actuation, constraints, and assignment of mountain and valley folds in origami are also incorporated into the geometric formulation. The experimental results show that the proposed method is efficient and accurate. The method can successfully simulate a flat-foldable degree-four vertex, two different action origami, the bistable property of a waterbomb base, and the elasticity of non-rigid origami panels.

1 Introduction

Origami is the art of paper folding, and it can be used to transform a flat sheet of paper into a three-dimensional (3D) shape without the paper being stretched, cut, or glued. However, paper origami is relatively weak and has little industrial use. When a stiff material is applied in origami, the sheets are normally joined by hinges where bending occurs. Since the sheets themselves cannot be bent, this kind of folding structure is called *rigid origami*. Just as with paper origami, a small number of folds can be combined to make intricate designs in rigid origami. As such, rigid origami has many practical uses, such as applications of stents, space telescopes, wheels, batteries, meta-materials, and 4D-printing.

As the use of rigid origami has grown, it has inspired studies in the mathematics of folding. Many designs have been presented, but because of the complex nature of folding, many problems remain. There has been a surge in the general interest in theoretical modeling and simulation that can promote an understanding and the development of novel folding solutions. Simulating the deformation of the origami is im-

portant for conceiving, designing, and constructing practical structures. Because rigid origami structures are stiff panels connected by hinges, one way to model them is to treat each hinge as a type of mechanical linkage [1]. To ensure that configurations are valid and do not contain self-intersections, constraints are applied to the fold angles. There are also numerical approaches that use spring or truss representation and triangulated meshes [2] to approximate the deformations. Although numerical methods may be computationally expensive because a constrained optimization is required to establish angle constraints, such methods are sometimes necessary to achieve accurate results, especially when the elastic properties of panels are also being considered. These methods focus on ideal origami, i.e., origami using materials of near-zero thickness, like paper. Nevertheless, thickness affects the folding behavior of a material and is not negligible in most cases.

The folds in a sheet of near-zero thickness are as simple as creases. However, the fold lines in a thick material have more complicated configurations, and they may not even be located at the same height along the thickness of the material. One example of a non-zero-thickness, single-line fold is a door hinge, which is always installed on the pull side of the door. Therefore, when there are both mountain and valley folds in a pattern, some of the fold lines are located on one side of a sheet while other folds are located on the other side. Various techniques [3] have been proposed to accommodate the thickness of materials. One way of implementing thick origami is to extend the same kinematic model that is used in near-zero-thickness patterns [4] to include thickness, for example, by offsetting panels from the original plane [5]. However, these methods are not always successful for typical rigid origami mechanisms with interior vertices, and they often require that the input surfaces are not flat. To develop thick origami, the finite element method (FEM) can be used as the simulation tool, but it is computationally expensive and, in general, is useful only in simple folding scenarios. Moreover, it is unable to easily preserve the assignment of mountain and valley folds. When a structure cannot make a sharp bend (as are possible with a creased idealization), the hinge can be modeled as a shallow cylindrical segment [6]

or a smooth fold [7] (as opposed to creased fold). The approach models the bent region to exhibit higher-order geometric continuity. The simulation of kinematic response is enabled by a non-linear and constrained optimization based on a generalization of Newton's method.

Although optimization methods perform thick origami simulations, the computations of these methods are expensive, and the thickness of the material is not directly considered. The challenges of simulating thick origami have motivated the present work to develop a simulation tool that can be efficient while accommodating the thickness of the material and the rigidity of the panels. Recently, the method of Geometric-Driven Finite Element (GDFE) [8] has been developed to analyze problems that primarily focus on shape deformation. This geometry-based method treats geometric actuation as inputs and geometric changes as outputs without having to convert the geometric variations into equivalent stresses and strains, as is the case with a traditional FEM.

The process of folding origami has usually been modeled by using the equations of kinematics. This kind of process is often referred to as the study of the "geometry of motion." However, kinematics is difficult to be generalized to consider the different properties of thick origami, such as the thickness or elasticity of the material. The objective of the present research is to use a geometry-based method to develop a general simulation of a thick material while maintaining the efficiency of origami kinematics. To achieve this objective, origami actuation, constraints, and the assignment of mountain and valley folds in the geometric formulation must be incorporated. The contributions of this paper are summarized as follows:

1. A framework is developed for the simulation of thick origami, which can automatically generate a geometric finite mesh from the origami pattern using different types of elements to represent the hinges and the panels, and can achieve real-time computations.
2. The actuation and folding based on the assignment of mountain and valley folds are realized by a geometry proximity function and a geometry projection operator.
3. To ensure that the configurations are valid, constraints on the solution space are incorporated in the projection operator without any additional burdens being imposed on the computation.

The experimental results verify the proposed method and demonstrate that it can simulate the folding of origami of arbitrary pattern, topology, and shape.

Some results of this paper were presented in a conference [9]. To be comprehensive, this journal version has provided more detail in the specific procedure applied to the process, given more detailed description of limitations or bounds on the approach, done some comparisons with existing physical models from the literature, and added a discussion to thoroughly explain the setting of the method.

The paper is organized as follows. The rest of this section outlines related works. Section 2 gives an overview of the geometric framework and its fundamentals. Sections 3 and 4 present the geometry proximity function and the geometry projection operator. The experimental results are given in Section 5. Section 6 discusses the settings and the practical issues, and the paper concludes in Section 7.

1.1 Related works

Origami simulation provides an understanding of the structures of origami models and can be used as tools for iterative design. Therefore, it is very important to users who apply origami to practical purposes. There are diverse approaches for origami models, and there are different classifications of models. This paper will emphasize differences in terms of the types of input/output of the deformation model. For this purpose, the classification proposed by Bowen et al. [10] is applied. That is, deformation models are categorized as kinematic, dynamic, analytical, and numerical.

Kinematic models are the most common because of their similarity to the nature of the rigid origami mechanisms – for example, spherical mechanism kinematics [11]. Because the panels are considered rigid, which means that the complexity of the model is reduced, kinematic methods can quickly converge to solutions. However, as aforementioned, kinematic models must be modified when the thickness or the properties of the material causes folds to be smooth instead of creased. For example, the offset crease technique [12] converts the original creases into two parallel symmetric folds that must stay the same when rotated. This technique results in a highly complicated model with a complex relationship that must be maintained [13].

Dynamic models are similar to kinematic models, but they approximate the hinges via torsional spring-dampers to account for material stiffness and damping [10]. The deformation is simulated by the force or torque inputs. However, problems of explicit integration schemes in dynamic models arise if the step sizes are too large. When simulating the elastic behavior of origami is also necessary, the panels can be modeled using plate theory [14]. Bar and hinge models [15] are also used to simulate non-rigid origami structures. With the help of graphics processing units, Ghassaei et al. [16] applied compliant constraints to guide the folding of an origami model, which can achieve an interactive speed that is compensated for by its accuracy.

Assuming specific beam geometries, analytical models can account for different hinge configurations, variable curvatures, or even elasticity [17]. These approaches explore a unit cell or a portion of the pattern empirically, which suits one specific origami pattern very well. However, these approaches cannot be readily extended to other origami systems or more complex geometries. Numerical methods, particularly the finite element (FE) model, discretize the system into smaller and simpler portions [18]. An FE model can determine the mechanical behavior of a model as a result of applied forces and represent the hinges directly as flexible materials. Alternatively, Tachi [19] derived a set of linear equations from the kinematics of rigid origami, with the fold angles considered as variables to represent the configuration of an origami model. The folding motion is numerically calculated using a linear approximation of constraints by single

vertices. The resultant trajectory is constrained by projecting the variables onto a feasible region of angular movement.

To summarize, kinematic and dynamic models are fast, but their use cannot be easily extended to general scenarios as can be done with elasticity and smooth folds. Analytical and numerical models are versatile in many aspects, yet they are generally created for relatively simple folding scenarios or small portions of the overall design. Otherwise, the computation is slow. In terms of rigid panel assumption, it is already considered in kinematic/dynamic models by representing the panel as a linkage, but this requires analytical/numerical models to simulate the rigidity through different material properties. There is a need to reach a compromise among these model types. This compromise should be computationally efficient to enable a full investigation of different families of origami shapes, particularly during the development of designs.

2 Geometric Simulation for Thick Origami

The FEM takes loads as input and stresses and deformations as outputs by solving a global system of equations that is generated from the element equations. While the FEM can theoretically provide a full understanding of origami design, it is computationally expensive due to the use of partial differential equations (PDE) and integral equations, the dynamics and large deformations in origami, as well as the possible non-linearity of material properties. These problems motivate this research to apply the principles in kinematics to FE models and present a geometry-based framework that is both versatile and efficient for origami simulation. The basic idea is to develop an FEM for which both its inputs and outputs are positions (which makes it similar to kinematic models), such that it can bypass the expensive computation of PDE and integration.

The framework relies on the concept of shape optimization [8]. Similar to FEM, it subdivides the whole model into smaller and simpler FEs. After knowing a current shape and defining the desired target shape of an element, a *geometry proximity function* can be used to measure the difference between the two shapes and deform the current shape into the target shape. Different elements have different properties and different shape transformations, depending on where they are located on the origami pattern (i.e., panels or hinges). Based on their configurations, the deformations and constraints are applied to each element through a *geometry projection operator*. The element equations in their geometric form are then assembled into a global system to compute the shape of the whole model. This is a unified framework that can handle origami constraints, thickness, and elasticity in the same formulation. This way, the computation is efficient and the implementation of the method is relatively simple. The present study presents the first time in which a geometry-based FEM has been applied to origami simulation. In addition, the framework provides a user-friendly interface that takes an arbitrary two-dimensional (2D) origami pattern as the input and automatically generates the finite mesh for the simulation, by which the hinges and panels are modeled dif-
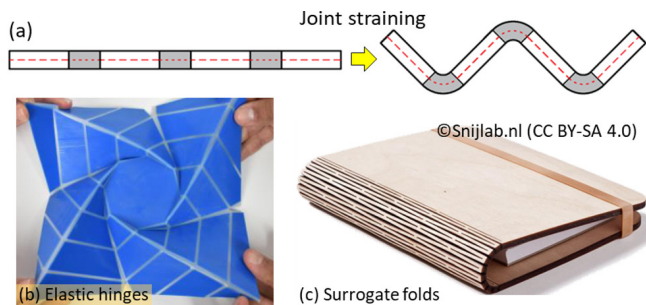
Fig. 1. (a) A compliant mechanism is based on the straining of joints [3]. Some examples include (b) using an elastic material at the joint area [20] and (c) using surrogate folds in a monolithic sheet.

ferently. The details are presented in the following subsections, starting with a discussion of the compliant mechanism this paper focuses on.

2.1 Compliant mechanism – strained joint

There are different compliant mechanisms [21] and thickness-accommodation techniques [3] to apply origami to engineering materials, including the tapered panel, offset panel, hinge shift, doubled hinge, rolling contacts, membrane, and strained joints. These techniques have unique sets of pros and cons in terms of design complexity, degrees-of-freedom, extension from zero-thickness patterns, etc. While most techniques generally require an assembly step and do not have a flat surface in their unfolded state, the strained joint technique (SJT) [22] is a compliant mechanism based on the straining of joints (Fig. 1a), so that it can be applied on a flat or even a monolithic sheet, thus easing its fabrication. This paper focuses mainly on the simulation of the SJT.

To allow the straining of joints, the joint areas between the rigid panels need to be flexible. This can be done by using elastic materials [20] (Fig. 1b), surrogate folds [23] (Fig. 1c), or sandwiched structures [24], etc. By putting rigid materials at the panels and elastomers at the hinges, folding can be achieved through the bending of elastic materials. A surrogate fold is a compliant joint that has a specific geometry to reduce the stiffness of the material in one or more particular directions, thus allowing it to be bent. When both the elastic and rigid materials are sandwiched at the joint area, the rigid material can also control the direction and the amount of bend. In any cases, bending occurs at the joint area, with both compressive and tensile strains. The SJT assumes that the thickness of a material is constant at the panels and hinges, as well as between its unfolded and folded states.

2.2 Geometric mesh of origami

Although it has been studied for a long time, the creation of FE meshes remains a challenging task. This is because FE mesh is not only a representation of the sub-domains but is also a key factor in geometry conformity, numerical complexity, and – more importantly – the analysis accuracy. A good mesh generation should apply physics based on an understanding of how things change. For origami structure, it
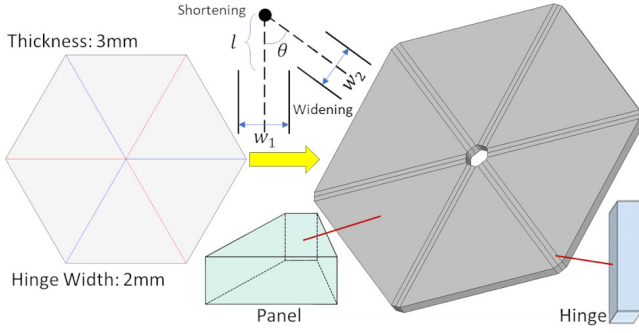
Fig. 2. The geometric mesh of thick origami is automatically generated from the 2D origami pattern with the given assignment of mountain and valley folds, thickness, and the number of hinge subdivisions.

is composed of panels and hinges, which exhibit different deformation behaviors during folding. Thus, they should be modeled differently. As origami sheets are 2D patterns with a particular thickness and the SJT is based on bending at the hinges, this paper constructs the volumetric mesh of origami via n-sided prisms, though n might be different for panels and hinges depending on the geometry of material. Bending can be approximated by scaling the sizes of the top and bottom faces of the prisms at the hinges. Because the straining of joints can be realized by different methods, the modeling of hinge here only aims at replicating the bending behavior of the joint rather than its exact geometry.

Specifically, the input of this framework is a 2D origami crease pattern (Fig. 2 left), which can be present in the form of polygonal mesh as defined by an STL/OBJ file or modeled by a freehand drawing tool within the interface. The assignment of mountain and valley folds can also be imported together with the pattern file, or they can be specified manually by the user. After the user defines the thickness as well as the width of hinges based on the material being used, the framework automatically generates the geometric mesh of thick origami. First, a widening operation is carried out on each hinge to set the width, and the width is then subdivided based on the user input value. Second, to convert each fold line into a compliant hinge attached to exactly two adjacent panels, the fold lines that merge at vertices are decoupled. This can be done by shortening the hinges to prevent overlapping between the widened hinges. The shortening length (l) is based on the width of the hinge (w_1) and the width of its adjacent hinge (w_2), as well as the angle between them (θ):

$$l = \frac{w_1}{2sin(A)} \quad \text{where} \quad A = \frac{sin\theta}{w_2/w_1 + cos\theta}. \quad (1)$$

This also results in a hole at the intersection of the hinges. Third, the thickness of the material is introduced to the 2D pattern creating volume. This is basically an extrusion operation, but it creates a volumetric mesh constituted by a set of prisms. The final result is shown on the right-hand side of Fig. 2. The whole finite mesh generation process is intuitive and automatic. The prisms created for hinges and panels have different shapes and sizes, so that they can reflect dif-
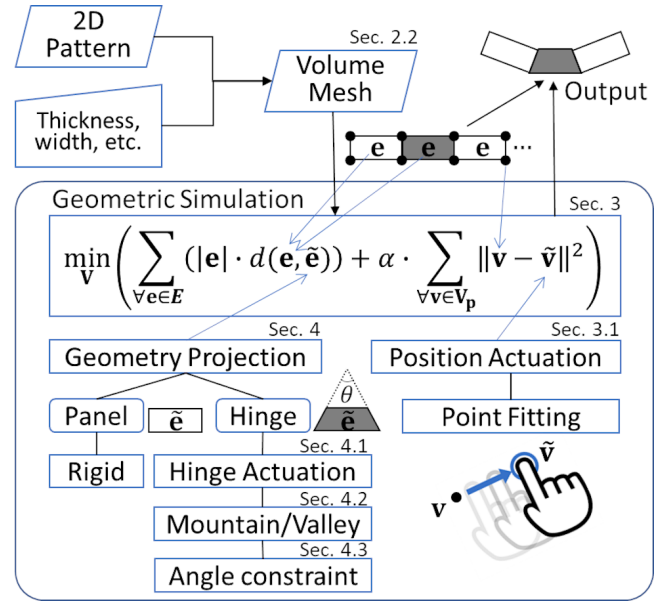
Fig. 3. A flowchart of the proposed geometric simulation framework.

ferent behaviors and be simulated differently, respectively.

3 Geometry Proximity Function

FE models are based on mechanics that take forces or displacements as inputs. In origami, the pattern is designed such that the mechanism of each portion has a unique purpose. For example, the creases bend in a defined direction, and the panels are meant to stay rigid. In other words, the deformed geometry of different portions can be estimated in certain ways. Since origami problems are defined by geometry, it is not necessary to convert the position input to the equivalent forces for stress-strain analysis. Instead, a geometry proximity and optimization can be applied to the FE formulation, which can directly consider the position. To allow the FE method to take positions as input and output positions, a geometric formulation needs to be developed for origami. The formulation must be fast, stable, and controllable so that it can be applied to various designs and used in an interactive environment. This section presents a geometry proximity function developed for such a purpose. A flowchart of the proposed framework is shown in Fig. 3.

3.1 Geometric approximation for strain energy

When an external force is applied to a body, the dimensions of the body change. The ratio of this dimensional change is the strain, which is a description of deformation excluding rigid-body motions. by modeling this physical phenomenon geometrically, it can be used to measure the "distance between the differential of deformation and the rotation group" [25]. In other words, a geometric model for minimizing the strain energy can minimize the difference between the deformed and original shapes and compute the optimal orientation between them. The overall deformation of the whole body is defined when the total strain energy of the

system is minimized. This work bases the development of the geometry proximity function on this principle.

Let the geometric mesh of origami be $\mathcal{M} = (\mathbf{V}, \mathbf{E})$, where $\mathbf{V}$ and $\mathbf{E}$ are the sets of vertices and elements. Each element $\mathbf{e}_n \in \mathbf{E}$ is an n-sided prism that has $2n$ vertices (i.e., $\mathbf{e}_n = [\mathbf{v}_1 \; \mathbf{v}_2 \; \dots \; \mathbf{v}_{2n}]$ with $\{\mathbf{v_i}\} \in \mathbf{V}$). Note that n could be different for every element in the mesh, and the list data structure is used to store the vertices in an element. The subscript n in $\mathbf{e}_n$ will be omitted in the rest of the paper for simplicity. It is assumed that the target shape of an element can be computed in a particular deformation instance, and it is also described by $2n$ vertices as $\tilde{\mathbf{e}} = [\tilde{\mathbf{v}}_1 \; \tilde{\mathbf{v}}_2 \; ... \; \tilde{\mathbf{v}}_{2n}]$. The shape proximity function is defined by measuring the difference between the current and the target shapes of all elements:

$$E = \sum_{\forall \mathbf{e} \in \mathbf{E}} |\mathbf{e}| \cdot d(\mathbf{e}, \tilde{\mathbf{e}}), \tag{2}$$

where $d()$ is the function used to measure the difference between the input shapes, and $|\mathbf{e}|$ is the volume of $\mathbf{e}$ to balance the effect of the element's size. Measuring the difference between 3D shapes and optimizing it would be a nontrivial problem because the orientation, position, and shape of the elements contribute to the function. To minimize the computational complexity of the optimization, the formulation needs to be carefully defined such that the factors can be uncoupled or solved separately. Three aspects are considered:

1. A centering matrix ($\mathbf{C}$) is applied to both shapes, thus shifting their centers to the origin so that the comparison is invariant to translation, and the effect of their absolute position is removed. The centering matrix has a size of $2n$-by-$2n$ and is defined as a matrix with all the diagonal elements as $\left(1 - \frac{1}{2n}\right)$ and all the non-diagonal elements as $\left(-\frac{1}{2n}\right)$. Multiplying this matrix by any vector has the same effect as subtracting the mean of the components of the vector from every component.

2. Because the current and optimal shapes of an element have defined one-to-one correspondences, the optimal orientation (i.e., rotation $\mathbf{R}$) can be pre-computed efficiently for every element in each iteration so that the optimization can focus only on the shape difference.

3. There are various ways (e.g., Hausdorff distance) to measure the difference between 3D shapes, but some of them may not have a closed-form expression or could result in a nonlinear formulation. To allow the optimization to be solved in a polynomial time, the Frobenius norm is used to compute the distances between the vertices of the element.

As a result, the geometry proximity function used for the FEM is formulated as

$$E = \sum_{\forall \mathbf{e} \in \mathbf{E}} |\mathbf{e}| \cdot ||\mathbf{C}\mathbf{e} - \mathbf{R_e}(\mathbf{C}\tilde{\mathbf{e}})||_F^2. \tag{3}$$

To minimize this function, its derivative is set to zero, which results in a system of linear equations:

$$(\mathbf{A}^\top \mathbf{A})\mathbf{V} = \mathbf{A}^\top \mathbf{B}, \tag{4}$$

where $\mathbf{A}$ is the global matrix that is constructed by all the centering matrices ($\mathbf{C}$), and $\mathbf{B}$ are the constant terms that come from $\mathbf{R_e}(\mathbf{C}\tilde{\mathbf{e}})$. Both are multiplied by the weights $|\mathbf{e}|$. In the conventional finite element method, where the stiffness matrix is used to describe the material property, the matrix must be updated in each deformation state to reflect the change in the material configuration, taking a long time in computing. In this geometric formulation, the global matrix $\mathbf{A}$ is assembled only by the centering matrices $\mathbf{C}$, which are always the same regardless of the deformation state – the shape changes are controlled through the target shapes $\tilde{\mathbf{e}}$ in the matrix $\mathbf{B}$. Therefore, the matrix $\mathbf{A}^\top \mathbf{A}$ can be prefactorized and reused for all iterations, and thus this system of linear equations can be solved multiple times efficiently. There are also other methods that model the strain energy of SJT, like applying spatial structures to consider thickness in a bistable interior vertex [26], but none can have such property.

To apply this geometry-based optimization to the simulation of origami, it must be able to consider the actuation of folding, mountain/valley folds, and angle constraints. When origami is folded by external actuation (e.g., by using one's hands to pin one end down while moving the other), it can be modeled by geometric constraints. One way to model this actuation is to add a position target, and the other way is through the bending of the hinge. The latter method is a type of geometry projection, which will be discussed in Sec. 4.1, while the former is discussed presently.

3.2 Actuation – position

A folding operation involves dragging one or more points to new positions such that the origami is deformed as desired. Intuitively, it can be modeled by hard position constraints. However, enforcing a point to be exactly located at a position is not how origami is folded in practice. Due to the kinematic constraints of origami, one would push the material and let the origami deform on its own. An exact position can be defined if all the kinematic relationships are mathematically well-defined, but it is difficult when the pattern is complicated and when the material is relatively thick. Therefore, the position actuation is not modeled by hard constraints. Instead, a fitting algorithm is applied here.

Let $\mathbf{V_p}$ be the set of points selected and dragged to new positions, where $\mathbf{V_p} \subset \mathbf{V}$. The points $\mathbf{v} \in \mathbf{V_p}$ are attracted towards their target positions $\tilde{\mathbf{v}}$, and the fitting objective function is defined as:

$$E_{pos} = \sum_{\mathbf{v} \in \mathbf{V_p}} ||\mathbf{v} - \tilde{\mathbf{v}}||^2. \tag{5}$$

After that, the overall energy to be minimized is the sum of the two functions:

$$\min_{\mathbf{V}}(E + \alpha \cdot E_{pos}), \tag{6}$$

where α is the weighting required to control the rate of response to the actuation. If it is too small, the folding process will be slow. If it is too high, the material will stretch. It is normally set as 1 at the beginning of the process, and its value decreases to 0 as the optimization converges. During the simulation, the user can continuously update the target positions according to the deformation, similar to the physical situation. The user can also remove the fitting at any time.

Both E and E_{pos} have a similar structure (distances from actual and target positions of vertices) so that they can be combined into one formulation. The difference between them is how the target positions are defined. The target positions in E come from the element shape $\tilde{\mathbf{e}}$ based on the deformation of materials, whereas those in E_{pos} are defined by the dragging of the vertices by the user into new positions. By comparing it with solid mechanics problems, E accounts for the internal strain energy, and E_{pos} represents the externally applied load.

4 Geometry Projection

In the previous section, it is assumed that the optimal shape of an element is known during deformation. This section will discuss how the shape is estimated by a geometry projection operator. For example, if an element is supposed to be rigid, this operator takes its original shape as the optimal shape ($\tilde{\mathbf{e}}$) and projects that onto its current shape ($\mathbf{e}$). The optimal orientation ($\mathbf{R}$) can be found by first obtaining the affine transformation ($\mathbf{T}$) via the equation $\mathbf{Te} = \tilde{\mathbf{e}}$ using a least square method and then extracting the rotation component by $\mathbf{R} = \mathbf{UV}^\top$, where $\mathbf{U}$ and $\mathbf{V}$ are the matrices from the singular value decomposition (SVD) of the affine transformation (i.e., $SVD(\mathbf{T}) = \mathbf{U\Sigma V}^\top$). Besides rigid elements, this operator can be applied to model the actuation, the assignment of mountain and valley folds, and the angle constraints, thus resulting in a general and unified framework for origami simulation. As the optimization itself minimizes the total strain energy based solely on the given target shapes, the selection of the target shape is critical, as it determines the final deformation. Therefore, the target shapes must be carefully defined to comply with solid mechanics. For example, the volume of a panel element should be conserved, the deformation of a hinge element should obey bending theory, and there must be no self-intersections between the elements. In this paper, the target shapes are computed by projecting the corresponding current shapes onto the shape space that satisfies these criteria. The details of each projection are given presently.

4.1 Actuation – hinge

The position actuation was presented in Sec. 3.2 to mimic the physical folding process via external directional forces. When the force is applied as a moment to a hinge, or when the hinge is the active material that causes the deformation (e.g., 3D printed origami [17]), the actuation should be modeled according to the rotation of the hinge. This
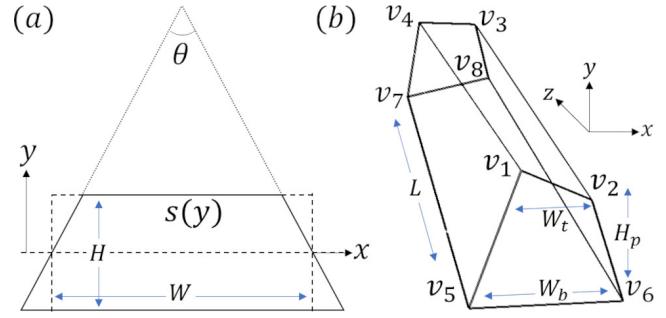
Fig. 4. (a) A hinge element is bent linearly by an angle θ shown in the front view. (b) A passive hinge can be distorted irregularly during deformation.

framework models hinge actuation by computing the optimal shape for a hinge element with a desirable degree of bending based on bending theory. Given a specific bending angle (θ), a hinge with a width W is deformed such that the angle between the normal vectors at their two ends is equal to θ. For the neutral axis located in the middle of the thickness (H), the curvature of the bend is $\kappa = 1/(r + 0.5H)$, where r is the bend radius. The bend can be expressed by the arc equation:

$$W = (r + \frac{H}{2})\theta. \tag{7}$$

When the elements of the hinge are small enough, the deformation can be approximated linearly (i.e., from a rectangular shape transformed into a trapezoidal shape). The basic purpose of the transformation is to scale the width of the element differently along the height dimension.

Specifically, the hinge element generated as described in Sec. 2.2 is a four-sided prism in the form of a rectangular bar (width $W \times$ height $H \times$ length L) in its undeformed shape. For the optimal shape to be computed intuitively, the prism must always be aligned with the coordinate system before any transformation is done. That is, the width and the thickness (height) of the prism are aligned with the x- and y-axes (Fig. 4(a)), and the length is aligned with the z-axis, which is also the axis of rotation. Under this configuration, the scaling factor can be defined as a function of y:

$$s(y) = 1 - \frac{2y}{W} \cdot \tan(\theta/2). \tag{8}$$

The element is centered at the origin, meaning that this equation is valid both for tension and compression. The optimal shape ($\tilde{\mathbf{e}}$) of a hinge element, given any bending angle θ, can then be computed by multiplying the scaling factor by all its vertices (i.e., $x = x \cdot s(y)$), where x and y are the coordinates of the vertex.

4.2 Assignment of Mountain and Valley Folds

When a hinge does not actuate, it deforms in a passive way. For those hinges, it is important that the simulation takes into account the assignments of mountain and valley

folds, if they are specified. This is because that some SJTs produce hinges with different stiffnesses along the thickness to favor or allow one-directional folds. Moreover, an origami pattern can result in different folded shapes with different assignments [27]. This section details how the assignment is satisfied in the presented framework.

Similar to the physical case, a passive hinge bends freely in such a way that the edges align to a fold angle θ determined by the overall origami deformation. Therefore, its optimal shape should be updated such that the shape proximity function is minimized. However, unlike the actuating hinge based on which the final optimal shape is defined, the optimal shape of a passive hinge is unknown and changes occasionally. Although the deformed shape of passive hinges could be computed through the optimization of Eq.(2), they might be distorted randomly and might not even represent the shape of a hinge (e.g., Fig. 4(b)). As a result, the distorted shape would not be set as the optimal shape. To overcome this challenge, the distorted shape is used as a reference to compute the shape that is closest to a valid hinge shape. Then, the closest shape is set as the optimal shape. Specifically, the bending angle (θ) of a passive hinge is estimated based on the distorted shape, and then Eq.(8) is applied to obtain the optimal shape for every time instant. A simple and fast way to estimate the angle is to compute the width difference between the top and bottom sides along the height of the hinge:

$$\theta = 2\tan^{-1}\left(\frac{W_b - W_t}{2H_p}\right), \qquad (9)$$

where the width and height are computed based on the average lengths following the notation in Fig. 4(b):

$$
\begin{aligned}
W_t &= 0.5(\|v_1 - v_2\| + \|v_3 - v_4\|), \\
W_b &= 0.5(\|v_5 - v_6\| + \|v_7 - v_8\|), \\
H_p &= 0.25(\|v_1 - v_5\| + \|v_2 - v_6\| + \|v_3 - v_8\| + \|v_4 - v_7\|).
\end{aligned}
\qquad (10)
$$

It can be seen from Eq.(9) that the bending angle (θ) would be positive for a valley fold and negative for a mountain fold. Here, if the estimated angle of a passive hinge violates the assignment of mountain and valley folds, it would be set to a small value according to the hinge's assignment.

Even the optimal shapes ($\tilde{\mathbf{e}}$) of the passive hinges are updated at each iteration such that they affect only the constant term (**B**) in Eq.(4). Without changing the global matrix (**A**), the pre-factorization results can be reused, and thus, the framework can accommodate the change of optimal shapes efficiently thanks to the geometry-based formulation.

4.3 Angle constraints

Although a hinge enables bending, it is not a rotary joint that can provide arbitrary or infinite rotation. Therefore, the bending of a hinge should follow certain constraints, one of which has already mentioned – the bending process needs to be confined by the assignment of mountain and valley folds. Another restraint is the limit of the fold angle, e.g., θ_{max}.
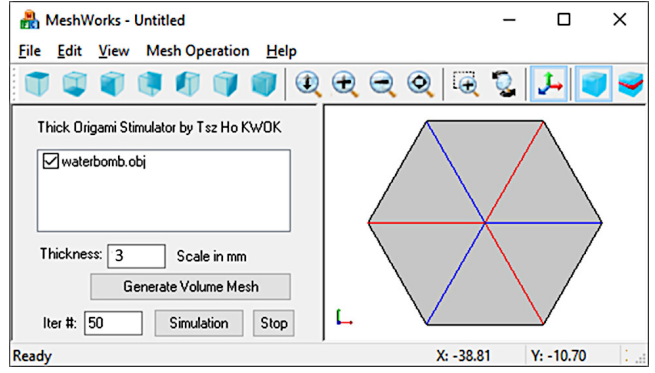
Fig. 5. User interface of the present simulator. In this screenshot, the pattern and its hinge information are imported, before generating the volume mesh (which was already shown in Fig. 2).

There are complaint mechanisms like a groove joint that have a maximum fold angle, and in any case, the fold angle cannot be larger than π due to the collisions between adjacent panels. Therefore, the range of bend angle is $(0 \; \theta_{max}]$ for valley folds and $[-\theta_{max} \; 0)$ for mountain folds. When there is no specified limit, θ_{max} is set as π by default. Once the bending angle of a passive hinge is estimated by Eq.(9), it is verified as being within the allowable range. If it does not fall into the acceptable range, the bend angle is projected back into the range. In this way, the angle constraints can be easily realized through the geometry projection without the need for constrained optimization.

The angle constraints presented here prevent only the local intersection between the panels at a hinge. This is not true in general because there could be global intersections (e.g., if the two tips of a shape resembling the letter 'C' were to touch each other). Collision checks for non-adjacent panels are required to detect global intersections, and this could be time-consuming. For the sake of computational speed, global intersection checks are not included in the current experiment. The local angle constraint serves the purpose generally.

5 Results

The proposed framework is implemented in VC++ and tested on a standard computer with a 64-bit Win-10 operation system, Intel (R) Core (TM) i5-1035G4 CPU @ 1.10GHz, and 8.00 GB RAM. The user interface is shown in Fig. 5. As mentioned in Section 2.2, the hinge information that is imported alongside with the mesh file defines one hinge per line in a format of edge ID, width, mountain/valley, and bend angle (optional). The bend angle is used when it is an actuated hinge (Section 4.1). The user only needs to specify the thickness of the material, and the volume mesh will be generated automatically. Although the CPU can support multi-core programming, this implementation is single-threaded, including the solver for linear equation systems, in order to demonstrate the capability of the geometric simulation. Because the geometric mesh was generated specifically for origami simulation, the number of elements is normally in the tens or hundreds for most origami patterns. With the
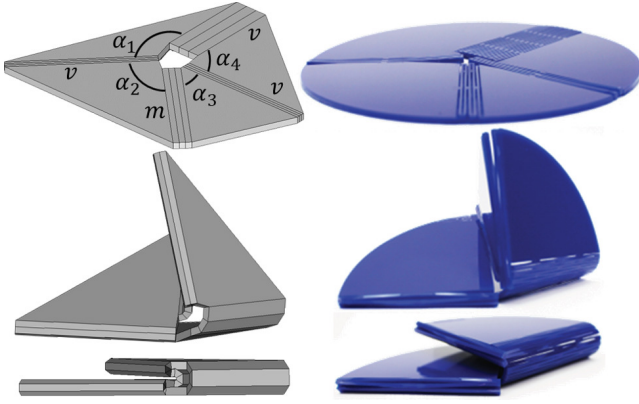
Fig. 6. The folding of a degree-four vertex origami: (left) simulated results and (right) physical results [3].

Fig. 7. The origami-inspired gripper is designed and fabricated in a 2D pattern [29] and can be actuated in its deployed state.

small mesh size and the simplicity of the geometric formulation, real-time simulation can be achieved with a single core. Among the cases tested, the slowest one is 3*ms* per frame, or 300 frame per second (FPS), which is much higher than the required rate for real time, i.e., 24 FPS. For the reader's information, the nonlinear bar-and-hinge method [28] takes 4 to 11 seconds in its examples.

Five selected examples are presented in this section to showcase different functionalities, including a degree-four vertex with flat-folded configuration, a gripper using action origami, an n-long linear chain with coupled action origami mechanisms, a waterbomb base with a bistable property, and a bar with elastic panels. The first two examples are compared with existing physical tests from the literature using surrogate folds. The last one is 3D-printed with an elastomer. For the sake of diversity, the third and fourth examples are tested using cardboard models to show the potential of the framework to be applied in other deformation mechanisms. The folding behavior of cardboard is dominated by the delamination of layers and buckling, and the underlying layers are incompressible. Although this is different from the SJT that is based on tension and compression, their behaviors share sufficient similarity for a demonstration. The exact modeling theory for cardboard models will be studied more thoroughly in the future, but some preliminary tests are shown here. The cardboard models have a thickness of 3*mm*.

5.1 Degree-four vertex

A degree-four vertex (D4V) is a single-vertex origami that is intersected by four hinges in the middle of the pattern (Fig. 6). It also has four sector angles: $\alpha_i, i = 1, \ldots 4$. A D4V is very important in the origami design due to two noteworthy properties. On the one hand, a D4V is flat-foldable if it satisfies the following condition borrowed from the Kawasakis theorem: $\alpha_1 + \alpha_3 = \alpha_2 + \alpha_4 = \pi$. This is an important feature that many origami designers try to include, as it can increase the portability and storage space of products. On the other hand, a D4V has only one degree-of-freedom (DOF) in its motion, which is the key to realize a single-DOF folding mechanism in an origami design. The
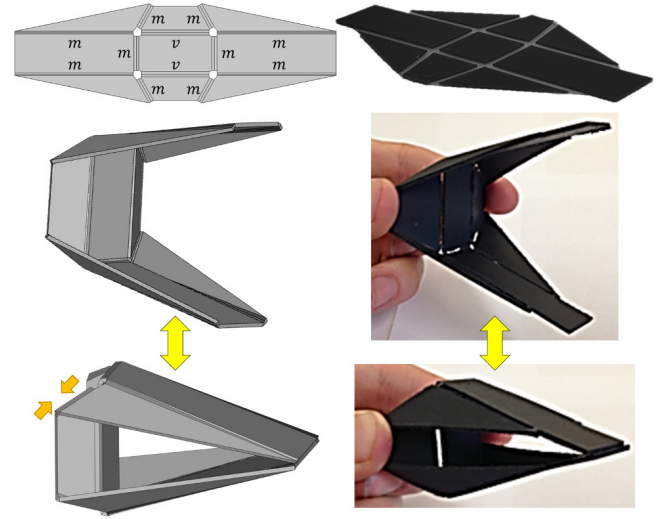
combination of these two features is very useful. If all the vertices of an origami model are flat-foldable D4Vs, the entire set of patterns could fold smoothly from its fully flat to fully folded states with a single DOF.

To test the proposed framework on this flat-foldable structure, the D4V design presented by Pehrson et al. [22] is used here (Fig. 6 right). The design is a circular pattern with a diameter of 152.4*mm* and $\alpha_1 = 135°$, $\alpha_2 = 90°$, $\alpha_3 = 45°$, and $\alpha_4 = 90°$. The physical model is fabricated with acrylic with a thickness of 3.175*mm* and the hinges are created by the SJT. Because of the material's thickness, to be flat-folded, the largest hinge should have a width of at least the sum of the widths of the other three hinges. In the design, the widths of the hinges are about 16*mm*, 4*mm*, 8*mm*, and 4*mm*. The same parameters are used to construct the simulation mesh, which is shown on the left-hand side of Fig. 6. For simplicity, the circular shape is not reconstructed – the arcs are replaced by straight lines – but this simplification will not affect the results or their accuracy. The arcs can always be drawn on top of the straight lines during or after the simulation if needed. Following the physical test [22], the intermediately folded and flat-folded configurations are simulated. The simulated and physical models are compared side-by-side in Fig. 6. The simulation runs in 1*ms* per frame and it takes 100 iterations getting to the flat-folded state. This example shows that the geometric framework can successfully simulate the flat-foldable mechanism with sharp bends and overlapping panels and hinges. The thickness of the material is considered, as indicated by the different heights of the folded shape, which would be missed by using near-zero-thickness techniques.

5.2 Gripper

The robotic gripper or forceps is widely applied in grasping and picking operations. Most of them require the assembly of several mechanical parts to enable motions. However, the parts often have a high complexity and they

are difficult to be cleaned. Oriceps are origami-inspired forceps devices developed by Edmondson et al. [30]. It can be fabricated with a single sheet of material, and the same design can be applied to both macro and micro scales. An oriceps pattern is shown in the top row of Fig. 7. Oriceps can be folded into a 3D shape based on the assignment of valley and mountain folds. The oriceps is an action origami that can be animated in its folded state. Its design is based on two spherical mechanisms that are coupled together. Pushing or pulling from the back causes the oriceps to open or close.

While the current designs are based on Shafer's "Chomper," a simulation framework would enable the exploration of various origami gripper designs for different applications. To test the proposed method, the pattern applied by Butler et al. [29] is inputted and is used to automatically generate the geometric mesh with 23 elements of which the thickness is $0.43mm$ and the hinge width is $1.52mm$. Besides the two hinges in the middle, which are valley folds, all other hinges are mountain folds. To fold the model into the deployed state, the hinges are set with target folding angles of around $50°$, except those at the top and bottom of the pattern (which are at the back of the folded forceps), which are set to a larger angle around $110°$. Under this configuration, the hinges are actuated, and the origami is formed into the 3D shape shown on the left-hand side of Fig. 7, which aligns well with the physical case that was fabricated by Butler et al. [29] using a 3D printer. In this deployed state, it can be further deformed through position actuation to mimic the actual use of the gripper. Through a comparison with the physical model, the actuation (and, thus, the action origami) can be simulated closely owing to the geometric simulation. The simulation runs in $2ms$ per frame and it takes 160 iterations to reach the closed position.

5.3 N-long linear chain

Another type of origami tested is a relatively complicated thick action origami – the n-long linear chain (Fig. 8), which is built on the foundation of the Shafer's "Frog's Tongue." A long chain can be designed with any number of spherical mechanisms that are coupled to one another with no loops. It is linear because all mechanisms (except the beginning and ending) share only two other mechanisms, but the orientation of each mechanism can be different. When one mechanism in the chain is actuated, all the others are moved together. Therefore, a small motion imposed at one end of the chain could result in a much larger motion for the whole origami. It could also be easily extended to "tree" mechanisms by attaching other mechanisms at the end of each branch, such as the "Attacking Cobra," by which the gripper design is used as the head and the chain design is used as the body and tail. The capabilities of converting and magnifying motions from one direction to another and transferring motions from one mechanism to others have many potential engineering applications when a material stronger than paper is used.

Similarly, the 2D pattern is inputted into the proposed framework and a geometric mesh with 60 elements is gen-
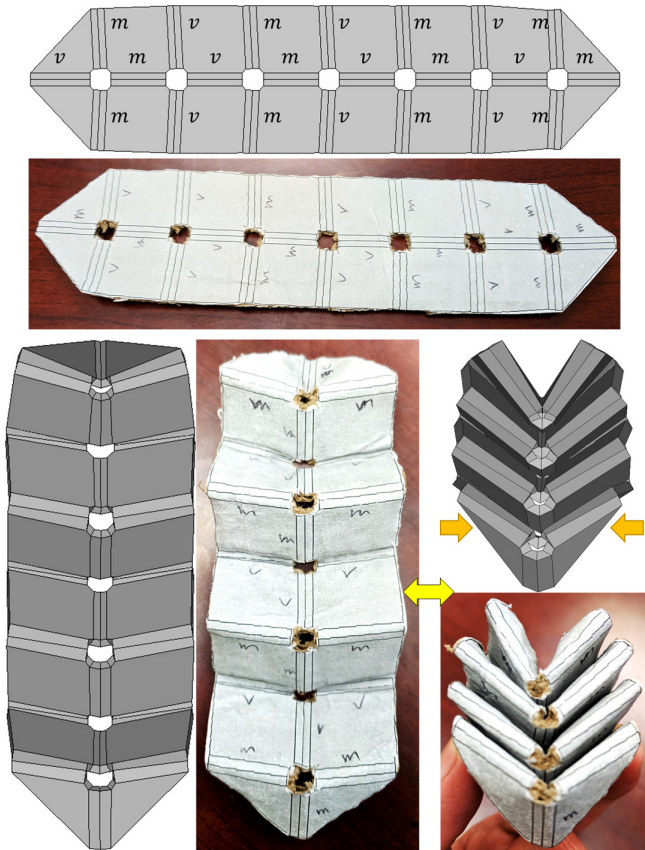
Fig. 8. An n-long linear chain fabricated in 2D can be deployed and actuated to change its longitudinal length by a small motion in the transverse direction.

erated: 44 for hinges and 16 for panels, as shown in Fig. 8. All the hinges are set to around $60°$ according to their own assignments of mountain and valley folds, and they are actuated to the deployed state. By controlling the horizontal displacement at one end, the structure transforms the type of motion from transverse to longitudinal. During the simulation, the transverse movement stops when the hinges are bent to around $180°$, due to the angle constraints. While the change in the transverse direction is small (from $4.5cm$ to $3cm$), the length in the longitudinal direction changes significantly (from $13cm$ to $4cm$). The same results are successfully simulated, which demonstrates the capability of the proposed geometric simulation to handle complicated relationships in action origami. The simulation runs in $3ms$ per frame and it takes 30 iterations to be fully compressed.

5.4 Waterbomb base

The origami waterbomb base is a fundamental origami fold that has spring-like and bistable properties [11]. It is a single-vertex origami that is intersected by six hinges in the middle of the pattern (Fig. 9). All hinges have the same length, and they are assigned with alternating mountain and valley folds. Because of its unique properties, it is useful in various applications outside of artistic origami. It has also been applied as a test bed for smart materials and actuators.
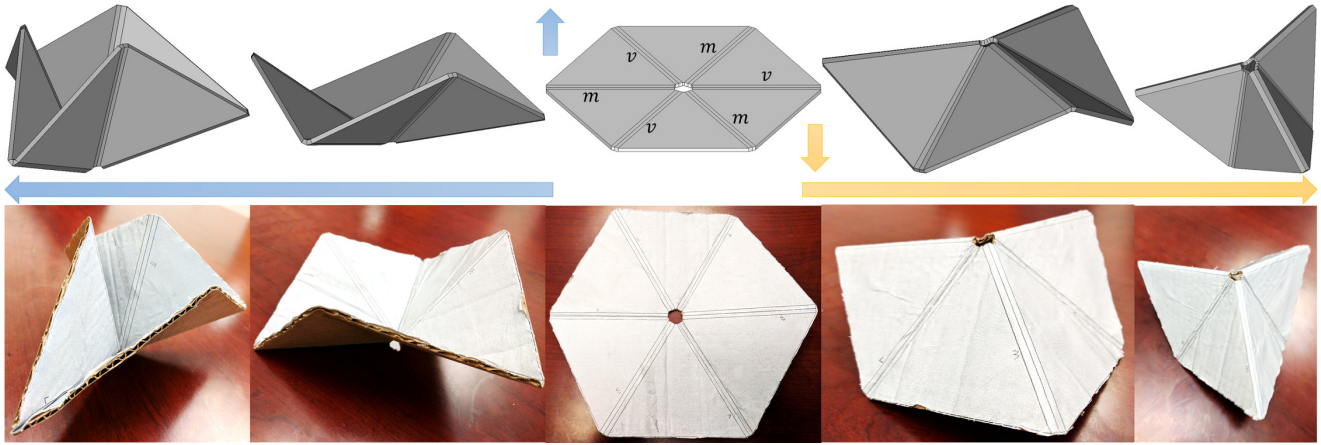
Fig. 9. The origami waterbomb base has a bistable mechanism. To the left, the origami is pushed up on the outside edge, and the middle vertex points downward. To the right, the vertex points upward when the origami is pushed down.

The term 'bistable' is used to refer to mechanisms that contain two stable equilibrium states. Besides, the origami waterbomb base also has an unstable equilibrium position, which is the plane shape shown in the middle of Fig. 9. A small disturbance causes the origami to leave this unstable position and reach one of the two stable positions. On the one hand, if there is a small upward push on the outside edge of the pattern, the vertex in the middle will quickly displace downward to get into the first stable position (see the left-hand side of Fig. 9). On the other hand, if the vertex is displaced so that the structure flattens back onto a plane and even surpasses the plane, the origami will snap into the second stable position (see the right-hand side of Fig. 9). This behavior is interesting because all of the folds still respect their own assignment of mountain valley folds throughout the bistable motion.

A waterbomb base's kinetic behavior can be simulated by completing kinematic and potential energy analyses [11]. FEA and virtual work analysis are also used to explore the locations of the stable equilibrium positions and the force-deflection response. However, the model is based on certain assumptions (e.g., symmetric configuration), meaning that developing analytical solutions to the general configurations would involve large numbers of variables and nested trigonometric functions. The proposed framework is applied to simulate for this waterbomb base as demonstrated in the top row of Fig. 9. Without defining the bend angles explicitly, all the hinges are deformed passively by giving a position actuation, and the mountain and valley folds eventually converge to different bend angles. The stronger the actuation is applied, the larger angles can be achieved. Similar results can also be observed in the physical experiments shown in the bottom row of Fig. 9. The simulation runs in 1*ms* per frame and it takes 250 iterations converging to one of the stable states.

In addition, to compare with the bistable behavior of existing physical models from the literature, the results of the prototype constructed by Hanna et al. [11] are reported in Table 1, which lists out the bend angles of the mountain and valley folds for each bistable position correspondingly. The

	Position 1		Position 2	
	θ_m	θ_v	θ_m	θ_v
Prototype [11]	$-82°$	$32°$	$-20°$	$55°$
Simulated	$-82°$	$24°$	$-17°$	$58°$

Table 1. Folded angles for bistable positions between the prototype [11] and the simulated result in this paper. θ_m and θ_v (in degree) are the angles of mountain and valley folds, respectively.

physical prototype was made of acrylic and metallic glass, where the acrylic glass is for the rigid panels and the metallic glass is for the hinges. It was fabricated in the first stable state (Position 1) and then moved to the second stable state (Position 2) by a tensile testing machine. In other words, the bend angles were predefined as at the Position 1, and it was to find out the resultant bend angles when the origami was moved to the Position 2. In order to mimic the condition in the present simulation, a hinge actuation is applied based on the bend angles at the Position 1, and then a position actuation is applied to move towards the Position 2. The simulated results are also reported in Table 1. Although the origami configuration is not exactly the same, similar behavior can be observed. For example, although in magnitude the bend angle of the mountain fold (θ_m) is set larger than that of the valley fold (θ_v) at the Position 1, it is inverse at the Position 2 due to symmetry between the two states. However, since the bend angles are not set according to the Position 2, there are larger internal forces in this position even it is a local minimum, and thus the resultant bend angles at the Position 2 are smaller in magnitude than that of the Position 1. From this result, although the energy associated with bistability may not be not explicitly captured, the positions of the bistable states are obviously captured.

5.5 Elastic panels

A major advantage of using a FE approach is that it can be easily extended to general cases. For example, if the pan-
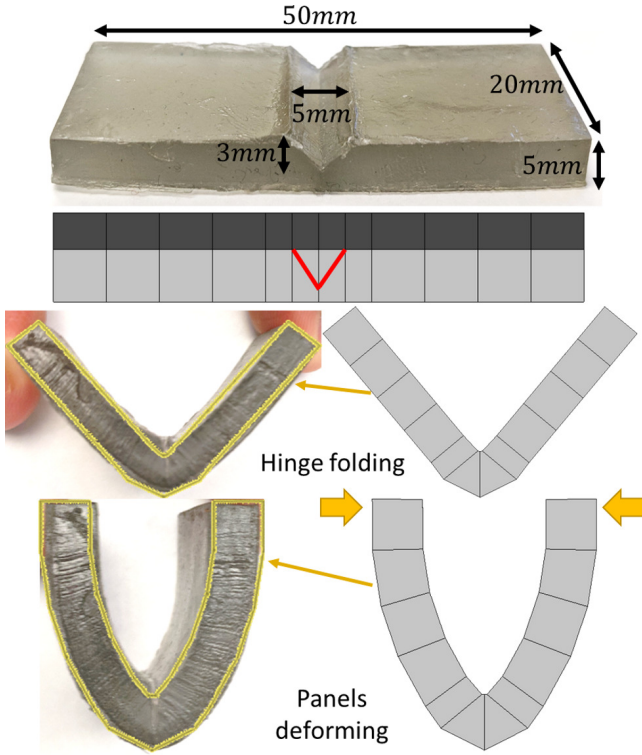
Fig. 10. An elastic bar with a V-shape groove joint at the middle is first deformed at the joint and then at the panels as bending continues. The highlights of the physical models are the contours of the simulated models.

Fig. 11. The relationship between different hinge subdivisions and widths on a $180°$ sharp bend.

els are not assumed to be rigid and their elasticity needs to be modeled, this can be realized by generating more subdivisions of the FEs for the panels. The models need to be significantly changed in kinematics or dynamics approaches. To provide proof-of-concept, a simple bar with a hinge in the middle is used as shown in Fig. 10. The main focus of this paper is rigid origami and the framework is developed to consider the rigid panel assumption. The present example only aims to demonstrate the possibility of extending the geometric framework to general situations. Further studies are needed to model the elastic panels and test the method in real general cases.

In this example, an elastic bar with a V-shape groove joint (a type of surrogate fold) at the middle is used as taken as a target object to test the method. It is made of the acrylate-based flexible material from ApplyLabWork (elongation $= 105 - 120\%$; shore $= 82 - 85A$), and the groove joint has a physical limit in bend angle of $90°$. Since the groove joint is a type of surrogate fold that deforms based on the SJT (see Sec.2.1), it can be modeled by hinge elements in this framework. A simulation mesh is generated correspondingly with the hinge in the middle and the panels on both ends. The hinge is assigned as a valley fold and is set to a maximum bend angle of $90°$. The main difference here is that the panels are represented by several elements in order to have more degree-of-freedom to deform. At the beginning of the bending action, the deformation is localized at the hinge just like the panels are rigid. When it reaches the maximum

angle for the hinge, the hinge cannot deform further. Then the panels start to deform elastically. The simulation results match with the physical ones very well. The simulation runs in $1ms$ per frame and it takes 280 iterations to have the panels also deformed.

6 Discussion

This section discusses some settings of the geometric simulation framework.

6.1 Hinge width and subdivision

Given the material thickness (H) and the bend angle (θ) of a hinge, it can be seem from Eq.(7) that the hinge width (W) is related to the sharpness of the bend, i.e., the bend radius (r), which is one of the design parameters that should be given to the system. It is similar to the calculation of bend allowance in sheet metal bending operations, where the sheet thickness, bend radius, and bend angle must be provided. For example, the hinges shown on the right-hand side of Fig. 11 have a thickness (H) of $0.5mm$ and a subdivision number of 8. For a bend angle $\theta = \pi$, when the hinge width $W = 0.8mm$, it yields a high curvature sharp bend (i.e., $r \approx 0$) with a coalescence of vertices. When $W = 1mm$, the curvature is lower with a larger bend radius and the folded structure is thicker. If either the hinge width or the bend radius is given, the system automatically calculates the other one. Otherwise, the bend radius r is set to zero by default to use the smallest width.

In terms of the hinge subdivision, it is known that for any mesh-based simulations, the higher the mesh resolution, the

smoother the simulation result but also the intenser the computation. Therefore, it is desirable to use the least number of subdivisions. To illustrate, assume there is only one element in the hinge region. If $W = 2$ and $H = 1$, the maximum angle θ_{max} is $2.2rad$ or $127°$, which is too small to be practical in an origami design. This is because when only one element is used to approximate the curved hinge linearly, it results in a significant error when the deformation is large. If the same hinge is represented by two elements, each of them has a size of $W = 1$ and $H = 1$. Correspondingly, the maximum angle θ_{max} for each element is $\pi/2$ or $90°$. The sum for the whole hinge is π, or $180°$, which is also the physical limit. Therefore, two elements are necessary for bend angles larger than $127°$. However, having more elements is desirable, especially when the bend is sharp. A demonstration of the subdivision number and the bend is given in Fig. 11. For an extreme case (a $180°$ sharp bend), different subdivisions give slightly different results due to the approximation. When there are two subdivisions, the bend is achieved by only two discrete linear lines, which yields a large error. When more subdivisions (e.g., 4 or 8) are present, smoother bends occur, and the curvatures are better approximated. Therefore, although two subdivisions are generally enough for most bends, more subdivisions should be used if the bend is large and sharp. As a balance between accuracy and efficiency, three to four subdivisions are suggested. The system could also automatically determine the number of subdivisions per hinge by the maximum bend angle θ_{max}.

6.2 Thickness

To explore how the thickness of material affects the results, the five-crease multiple-vertex origami used by Chen et al. [4] to make boxes (Fig. 2 of their paper) is taken as an example. The pattern is shown in Fig. 12, which has six vertices and each vertex is intersected by five hinges. Only the origami pattern is employed here for the testing, and the aim is not to compare the results. This is because different compliant mechanisms are applied: this paper focuses on SJT, but Chen et al. [4] converted the five-crease vertices to Myard (spatial $5R$) linkage with varied panel thickness.

Two thicknesses are tested: $H = 1mm$ and $H = 4mm$, and the results are also shown in Fig. 12. Apparently, both the 2D sheets and 3D shapes have quite a difference. From Eq.(7), the hinge width should increase with the material thickness. When $H = 1mm$, the width W should at least be $1.57mm$; and similarly $W = 6.28mm$ for $H = 4mm$. In other words, the thicker the material is, the larger the hinge width needs to be in order to achieve the same bend angle. With the changes in hinge width, the shortening lengths in Eq.(1) are also altered, as well as the residual holes. All these result in different 2D sheets. When the sheets are folded into boxes, the two panels adjacent to the mountain-fold hinge are put together and protrude in the inside volume. When the hinges are wider, the protruding parts are relatively shorter as the panels get smaller. However, they get bigger and more conspicuous as the material thickness increases, and the volume of the box is also reduced. Since the thickness of origami will
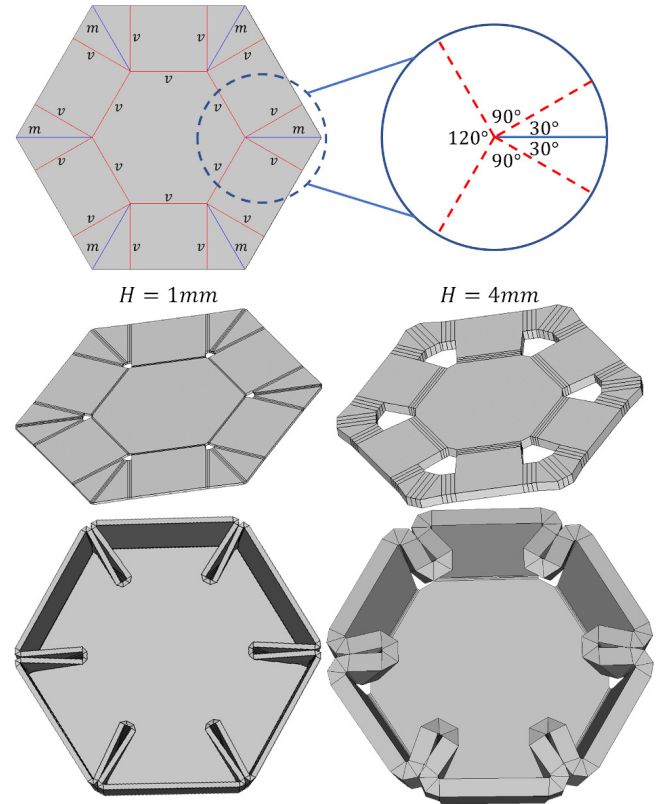
Fig. 12. Two thicknesses ($H = 1$ and $4mm$) are tested on a five-crease multiple-vertex origami [4] in making a box.

change the shape and the volume of the box, the modeling of it must take the thickness into consideration.

6.3 Target shape

In this geometric simulation framework, the deformation is basically controlled by the selection of target shapes. The efficiency of computation is also based on this parameter because the target shape $\tilde{\mathbf{e}}$ affects only the matrix $\mathbf{B}$ on the right-hand side of Eq.(4). Thus, the global matrix could be pre-factorized and reused. Each element (panels and hinges) yields a set of equations that are related to its vertices, and a vertex is shared by multiple elements, resulting in more equations than vertices. The linear system is thus overdetermined and solved by the method of least squares in the form of Eq.(4). Because of the use of least squares, this formulation is so robust that even when the target shapes of the neighboring elements are not compatible, it can still find an approximation to balance the difference by minimizing the geometrically approximated strain energy. As an illustration, if two elements have different thickness, the face shared by them would take the average thickness, and the overall shape would be like the diffuse necking in the tensile deformation.

In addition, although the geometry projection presented in Sec. 4 is based primarily on bending, it is not limited to bending and can be generalized. If a hinge were to exhibit behaviors other than bending, different theories could be used to define the target shape of the hinge. For example, if a hinge was stretched, its target shape should be set as

the stretched shape based on the Poisson effect and then the framework would stretch the hinge rather than bend it.

6.4   Fracture

With the measure of scaling factor in Eq.(8), the elastic or fracture strains of the material are possible to be incorporated to check for failures of the origami. The bending stress increases linearly away from the neutral axis until the maximum values at the top or bottom of the beam. The material fails when the maximum stress exceeds its tensile strength, or correspondingly when the strain exceeds its fracture strains (ε_t and ε_c, where t and c stand for tensile and compressive). Since strain is the percent elongation, which is defined as the ratio between the deformed length and the initial length, the limits of the approximated hinge strain can be defined in terms of the scaling factor:

$$1 - \varepsilon_c < s(\pm 0.5H) < 1 + \varepsilon_t.$$

To identify the point of fracture, the bend angle of every hinge is first obtained by Eq.(9), and then the scaling factor $s(\pm 0.5H)$ can be computed using Eq.(8). If the result is out of the above limits, the material fails at that time step.

7   Conclusion

This research is motivated by the observation that origami is commonly modeled by the geometry of motion. A geometry-based simulation framework for thick origami is presented in this paper. The present geometric simulation focuses on the shape deformation, and its inputs and outputs are also positions. The origami actuation, constraints, and assignments of mountain/valley folds are seamlessly incorporated by using a geometry proximity function and a geometry projection operator. This framework has been tested with various configurations of origami, such as a gripper action origami, a bistable waterbomb base, and a groove joint with elastic panels. The method is as generalizable as a conventional FEM, but it has the efficiency of kinematic models. The results of the geometric simulation are very promising for thick origami, and the simulation can be applied to the iterative design of thick origami. For example, flat-foldable origami can be used for many interesting applications. However, a flat-foldable design normally needs to undergo certain modifications and adaptions to be applied to thick materials. Although this method cannot be directly applied to create such origami, this simulation framework could be used in combination with a design iteration method to test various designs if they are flat-foldable. This will be the subject of future work. Similarly, this framework can also be used to test different design parameters (e.g., hinge width) and to explore the relationships among shape, geometry, pattern, and hinge properties.

Despite the encouraging results presented here, the framework, in its current state, has some limitations. First, it does not consider the interference of the origami itself or of other objects. If the pattern is not well-designed, the model might involve self-intersections. Although action origami (e.g., a gripper) is simulated, the loads that can be applied to the foreign bodies are unknown. In the future, stress recovery and contact simulation [31] can be incorporated in the geometric framework. Second, the current simulation of elastic panels is for 1D deformations only. More general deformations (e.g., the parasitic effect bending along a diagonal and forming dimples [32] or dents [33]) would require 2D or even 3D mesh subdivision. The mesh subdivision is currently defined by the designer. However, the geometric mesh of origami directly affects its accuracy and efficiency. To balance these parameters, it is preferred that an adaptive mesh subdivision is applied during the simulation so that only high-curvature areas are represented by fine mesh. Third, the present framework assumes the panels are rigid and not deforming, and thus only one material – the hinges – is deforming, so the material properties do not matter. This is because the inputs and outputs of the framework are positions, and it is just like stretching an aluminum bar and a steel bar to increase 50% of their length will both give a strain of 50%. However, it is only true when there is only one material deforming. If there are more than one material deforming or the hinges have different stiffness, the material properties must be considered. This can be realized by setting different target shapes, but more in-depth studies need to be done to find out how to set the target shapes for different materials, and it will be a future work. Fourth, the geometric analysis right down does not report the stress information. Since the deformation (i.e., the strain) is obtained, it is possible to extracted the stress from the displacements, just like the stress recovery in finite element analysis. However, the straining of joints could be realized by different methods (e.g., surrogate folds), the calculation of stress needs to consider the actual mechanism used to realize the SJT and maps the deformation from the hinge elements to the exact geometry of the joints. This would require a more thorough study and analysis to develop a proper correspondence and interpolation algorithm in the future.

References

[1] Demaine, E. D., and O'Rourke, J., 2007. *Geometric Folding Algorithms: Linkages, Origami, Polyhedra.* Cambridge University Press.

[2] Tachi, T., 2010. "Freeform variations of origami". *J. for Geo. & Graph.,* **14**(2), pp. 203–215.

[3] Lang, R. J., Tolman, K. A., Crampton, E. B., Magleby, S. P., and Howell, L. L., 2018. "A review of thickness-accommodation techniques in origami-inspired engineering". *Appl. Mech. Rev.,* **70**(1), pp. 010805–20.

[4] Chen, Y., Peng, R., and You, Z., 2015. "Origami of thick panels". *Science,* **349**(6246), pp. 396–400.

[5] Edmondson, B. J., Lang, R. J., Magleby, S. P., and Howell, L. L., 2014. "An offset panel technique for thick rigidly foldable origami". In ASME IDETC/CIE, p. V05BT08A054.

[6] Walker, M. G., and Seffen, K. A., 2019. "The flexural mechanics of creased thin strips". *International Journal of Solids and Structures, 167*, pp. 192 – 201.

[7] Peraza-Hernandez, E. A., Hartl, D. J., Akleman, E., and Lagoudas, D. C., 2016. "Modeling and analysis of origami structures with smooth folds". *Computer-Aided Design, 78*, pp. 93 – 106. SPM 2016.

[8] Kwok, T. H., and Chen, Y., 2017. "GDFE: Geometry-driven finite element for four-dimensional printing". *ASME. J. Manuf. Sci. Eng., 139*(11), pp. 111006–8.

[9] Kwok, T.-H., 2019. "Geometric simulation for thick origami". In Proc. ASME 2019 International Design Engineering Technical Conferences and Computers and Information in Engineering Conference, Vol. 5B, p. V05BT07A022.

[10] Bowen, L., Springsteen, K., Ahmed, S., Arrojado, E., Frecker, M., Simpson, T. W., Ounaies, Z., and von Lockette, P., 2017. "Design, fabrication, and modeling of an electricmagnetic self-folding sheet". *J. Mech. Robot., 9*(2), pp. 021012–13.

[11] Hanna, B. H., Lund, J. M., Lang, R. J., Magleby, S. P., and Howell, L. L., 2014. "Waterbomb base: a symmetric single-vertex bistable origami mechanism". *Smart Materials and Structures, 23*(9), p. 094009.

[12] Ku, J. S., and Demaine, E. D., 2016. "Folding flat crease patterns with thick materials". *J. Mech. Robot., 8*(3), pp. 031003–6.

[13] Cao, Y., 2017. "Rigid origami of thick panels and deployable membranes". Master's thesis, University of Oxford.

[14] Wei, Z. Y., Guo, Z. V., Dudte, L., Liang, H. Y., and Mahadevan, L., 2013. "Geometric mechanics of periodic pleated origami". *Phys. Rev. Lett., 110*, May, p. 215501.

[15] Zhu, Y., and Filipov, E. T., 2020. "A Bar and Hinge Model for Simulating Bistability in Origami Structures With Compliant Creases". *Journal of Mechanisms and Robotics, 12*(2), 02. 021110.

[16] Ghassaei, A. P., Demaine, E. D., and Gershenfeld, N., 2018. "Fast , interactive origami simulation using gpu computation". In Origami[7].

[17] Kwok, T.-H., Wang, C. C. L., Deng, D., Zhang, Y., and Chen, Y., 2015. "Four-dimensional printing for freeform surfaces: Design optimization of origami and kirigami structures". *J. Mech. Des., 137*(11), pp. 111413–10.

[18] Gattas, J. M., and You, Z., 2015. "The behaviour of curved-crease foldcores under low-velocity impact loads". *International Journal of Solids and Structures, 53*, pp. 80 – 91.

[19] Tachi, T., 2009. "Simulation of rigid origami". *Origami 4*, pp. 175–187.

[20] Stark, J., and Kalantar, N., 2018. An overview of fabrication techniques for single-assembly folding structures. Tech. rep., Texas A&M University, 06.

[21] Howell, L. L., 2001. *Compliant Mechanisms*. A Wiley-Interscience publication. Wiley.

[22] Pehrson, N. A., Magleby, S. P., Lang, R. J., and Howell, L. L., 2016. "Introduction of monolithic origami with thick-sheet materials". *Proceedings of IASS Annual Symposia, 2016*(13), pp. 1–10.

[23] L, D. I., P, M. S., and L, H. L., 2015. "Evaluating compliant hinge geometries for origami-inspired mechanisms". *ASME. J. Mech. Robot., 7*(1), pp. 011009–8.

[24] Butler, J., Pehrson, N., and Magleby, S., 2019. "Folding of Thick Origami Through Regionally Sandwiched Compliant Sheets". *Journal of Mechanisms and Robotics, 12*(1), 10. 011019.

[25] Chao, I., Pinkall, U., Sanan, P., and Schröder, P., 2010. "A simple geometric model for elastic deformations". *ACM Trans. Graph., 29*(4), July, pp. 38:1–38:6.

[26] Pehrson, N. A., Magleby, S. P., and Howell, L. L., 2018. "An origami-based thickness-accommodating bistable mechanism in monolithic thick-sheet materials". In 2018 International Conference on Reconfigurable Mechanisms and Robots (ReMAR), pp. 1–7.

[27] Saito, K., Tsukahara, A., and Okabe, Y., 2016. "Designing of self-deploying origami structures using geometrically misaligned crease patterns". *Proceedings of the Royal Society A: Mathematical, Physical and Engineering Sciences, 472*(2185), p. 20150235.

[28] Liu, K., and Paulino, G. H., 2017. "Nonlinear mechanics of non-rigid origami: an efficient computational approach". *Proceedings of the Royal Society A: Mathematical, Physical and Engineering Sciences, 473*(2206), p. 20170348.

[29] Butler, J., Bowen, L., Wilcox, E., Shrager, A., Frecker, M. I., von Lockette, P., Simpson, T. W., Lang, R. J., Howell, L. L., and Magleby, S. P., 2018. "A model for multi-input mechanical advantage in origami-based mechanisms". *ASME. J. Mech. Robot., 10*(6), pp. 061007–9.

[30] Edmondson, B. J., Bowen, L Aand Grames, C. L., Magleby, S. P., Howell, L. L., and Bateman, T. C., 2013. "Oriceps: Origami-inspired forceps". In ASME Smart Materials, Adaptive Structures and Intelligent Systems, p. V001T01A027.

[31] Zhu, Y., and Filipov, E. T., 2019. "An efficient numerical approach for simulating contact in origami assemblages". *Proceedings of the Royal Society A: Mathematical, Physical and Engineering Sciences, 475*(2230), p. 20190366.

[32] Walker, M. G., 2020. "Mechanics of generically creased disks". *Phys. Rev. E, 101*, Apr, p. 043001.

[33] Walker, M. G., and Seffen, K. A., 2018. "On the shape of bistable creased strips". *Thin-Walled Structures, 124*, pp. 538 – 545.